A very dark stellar system lost in Virgo: kinematics and metallicity of SECCO 1 with MUSE

G. Beccari, M. Bellazzini, L. Magrini, L. Coccato, G. Cresci, F. Fraternali, P. de Zeeuw, B. Husemann, R. Ibata, G. Battaglia, et al.

Monthly Notices
of the
ROYAL ASTRONOMICAL SOCIETY

MNRAS **465,** 2189–2197 (2017) doi:10.1093/mnras/stw2874
Advance Access publication 2016 November 8

A very dark stellar system lost in Virgo: kinematics and metallicity of SECCO 1 with MUSE

G. Beccari,[1⋆] M. Bellazzini,[2] L. Magrini,[3] L. Coccato,[1] G. Cresci,[3] F. Fraternali,[4] P. T. de Zeeuw,[1,5] B. Husemann,[1] R. Ibata,[6] G. Battaglia,[7] N. Martin,[6,8] V. Testa,[9] S. Perina[2] and M. Correnti[10]

[1]*European Southern Observatory, Karl-Schwarzschild-Strasse 2, D-85748 Garching bei München, Germany*
[2] *INAF – Osservatorio Astronomico di Bologna, Via Ranzani 1, I-40127 Bologna, Italy*
[3]*INAF – Osservatorio Astrofisico di Arcetri, Largo E. Fermi 5, I-50125 Firenze, Italy*
[4]*Dipartimento di Fisica and Astronomia, Università degli Studi di Bologna, Viale Berti Pichat, 6/2, I-40127 Bologna, Italy*
[5]*Leiden Observatory, Leiden University, Postbus 9513, NL-2300 RA, Leiden, the Netherlands*
[6]*Observatoire Astronomique de Strasbourg, Université de Strasbourg, CNRS, UMR 7550, 11 rue de l'Université, F-67000 Strasbourg, France*
[7]*Instituto de Astrofisica de Canarias, E-38205 La Laguna, Tenerife, Spain*
[8]*Max-Planck-Institut für Astronomie, Königstuhl 17, D-69117 Heidelberg, Germany*
[9]*INAF – Osservatorio Astronomico di Roma, via Frascati 33, I-00040 Monteporzio, Italy*
[10]*Space Telescope Science Institute, Baltimore, MD 21218, USA*

Accepted 2016 November 4. Received 2016 November 3; in original form 2016 July 6

ABSTRACT

We present the results of VLT-MUSE (Very Large Telescope-Multi Unit Spectroscopic Explorer) integral field spectroscopy of SECCO 1, a faint, star-forming stellar system recently discovered as the stellar counterpart of an ultracompact high-velocity cloud (HVC 274.68+74.0), very likely residing within a substructure of the Virgo cluster of galaxies. We have obtained the radial velocity of a total of 38 individual compact sources identified as H II regions in the main and secondary bodies of the system, and derived the metallicity for 18 of them. We provide the first direct demonstration that the two stellar bodies of SECCO 1 are physically associated and that their velocities match the H I velocities. The metallicity is quite uniform over the whole system, with a dispersion lower than the uncertainty on individual metallicity estimates. The mean abundance, $\langle 12 + \log(\mathrm{O/H})\rangle = 8.44$, is much higher than the typical values for local dwarf galaxies of similar stellar mass. This strongly suggests that the SECCO 1 stars were born from a pre-enriched gas cloud, possibly stripped from a larger galaxy. Using archival *Hubble Space Telescope* (*HST*) images, we derive a total stellar mass of $\simeq 1.6 \times 10^5\,\mathrm{M}_\odot$ for SECCO 1, confirming that it has a very high H I-to-stellar mass ratio for a dwarf galaxy, $M_{\mathrm{H\,I}}/M_* \sim 100$. The star formation rate, derived from the Hα flux, is a factor of more than 10 higher than in typical dwarf galaxies of similar luminosity.

Key words: H II regions – galaxies: dwarf – galaxies: star formation.

1 INTRODUCTION

SECCO[1] (Bellazzini et al. 2015a, hereafter B15a) is a survey aimed at searching for stellar counterparts of ultracompact high-velocity clouds (UCHVCs) of neutral hydrogen that have been recently proposed by different teams as candidate mini-haloes residing in the Local Group or its surroundings ($D \lesssim 3.0$ Mpc; Saul et al. 2012; Adams, Giovanelli & Haynes 2013, ALFALFA and GALFA-H I surveys, respectively). The only way to confirm the nature of UCHVCs as small gas-rich dwarf galaxies is to identify a concomitant stellar population that can allow us to constrain the distance to the system. Several groups have attempted this search, mainly using public archive data. On the other hand, SECCO is based on very-deep, homogeneous, wide-field imaging obtained with the Large Binocular Telescope (MtGraham, AZ), allowing a full quantitative characterization of non-detections (Beccari et al. 2016, hereafter B16).

In B15a, we identified a candidate faint and blue stellar counterpart to a UCHVC from the Adams et al. (2013, hereafter A13) sample (HVC 274.68+74.0). The spectroscopic follow-up of the

⋆ E-mail: gbeccari@eso.org
[1] http://www.bo.astro.it/secco

brightest source of the system, by Bellazzini et al. (2015b, hereafter B15b), showed that it is an H II region at the same velocity[2] of the cloud, $V_r = -128 \pm 6$ km s^{-1} (A13), hence physically associated with it. As detailed in B15b, having considered several different hypotheses, we concluded that the newly discovered stellar system, which we baptized SECCO 1, is (most probably) a star-forming and extremely gas-rich ($M_{\rm H\,I}/L_V \sim 20$) dwarf galaxy located in the Virgo cluster of galaxies. In particular, SECCO 1 likely resides within the substructure named a low-velocity cloud (LVC) whose members' radial velocity spans the range of $-400 \lesssim V_r \lesssim +400$ km s^{-1} (Boselli et al. 2014). The coarse metallicity estimate we obtained in B15b was suggestive of a system much more metal-rich than the typical dwarf of similar luminosity. Sand et al. (2015) confirmed our conclusions with independent data but did not provide an independent estimate of the metallicity. On the other hand, they identified a second small group of blue stars ∼2 arcmin north-east of the main body of SECCO 1, suggesting that the two systems are associated. In the following, we will refer to the original stellar system found by B15a as the MB of SECCO 1, and to the new group as its secondary body (SB). In B16 we showed that SB is indeed recognizable in our original SECCO images and that some additional blue sources possibly associated with SECCO 1 can be identified also to the east of the MB. Moreover, by comparison with very low surface brightness dwarfs also residing in Virgo, identified in the same images as SECCO 1, we were able to constrain any population older than ∼2 Gyr within SECCO 1 to have surface brightness significantly fainter than $\mu_V \simeq 27.0$ mag arcsec^{-2}.

Finally, Adams et al. (2015, hereafter A15) presented new H I observations that resolved the original HVC 274.68+74.0 cloud (that was seen as an individual entity of size 5 × 4 arcmin^2 at the 3 arcmin resolution of the ALFALFA survey) into an ≃1.75 × 1.25 arcmin^2 main cloud nearly centred on MB (AGC 226067), likely connected by a thin bridge to a smaller cloud (≃0.75 × 0.75 arcmin^2, AGC 229490) located ≃0.5 arcmin to the west of SB. A15 concluded that (i) with the revised estimates of the mass of the gas clouds, the gas-to-stellar-luminosity (mass) ratio becomes less extreme than that derived by B15b and S15, and more similar to the galaxies studied by Cannon et al. (2011), and (ii) SECCO 1 MB (AGC 226067), SB (which they call AGC 229491) and the nearby cloudlet AGC 229490 are three low-mass galaxies within the Virgo cluster having some kind of mutual interaction (see A15 for a detailed discussion, and Bekki 2015, for a theoretical analysis).

Here we present the velocity field and the metallicity of several H II regions in SECCO 1 MB and SB obtained with the Multi Unit Spectroscopic Explorer (MUSE) at the Very Large Telescope (VLT). Archival images data taken with the *Hubble Space Telescope* (*HST*) are used in support of our study. A thorough analysis of the full wealth of information contained in the MUSE and *HST* data is deferred to a future contribution, where we will discuss in depth the various hypotheses for the origin of SECCO 1. According to Mei et al. (2007), the Virgo cluster has a significant depth along the line of sight (the $\pm 3\sigma$ range is ∼4 Mpc). Hence, it should be kept in mind that the distance of SECCO 1 is not so tightly constrained by its membership to Virgo; the LVC probably lies slightly behind the core of the cluster (Mei et al. 2007). In the following, we adopt the conventional distance $D = 17.0$ Mpc, after Boselli et al. (2014) and consistent with A15.

[2] All the velocity values reported in this paper are heliocentric radial velocities (V_r).

2 OBSERVATIONS AND DATA REDUCTION

MUSE is a panoramic integral-field spectrograph able to acquire low-resolution spectra ($R = 2000 - 4000$, from the bluest to the reddest wavelength) in the spectral range 0.465–0.93 μm (Bacon et al. 2014). The adopted wide field mode (WFM) provides a field of view (FoV) of 1 × 1 arcmin^2, with a pixel scale of 0.2 arcsec pixel^{-1}. A total of 4 h of telescope time was allocated to the Director's Discretionary Time programme 295.B-5013 (PI: Beccari).

Two pointings were sufficient to sample the MB and the SB of SECCO 1. For each target, we acquired six exposures of 1000 s each. We used a simple dither pattern and applied a 90° offset to the derotator between each consecutive exposure, to improve the flat-fielding and to ensure a homogeneous image quality across the FoV. The average seeing during the exposures was 0.7 arcsec, corresponding to a measured full width at half-maximum (FWHM) of ∼3.5 pixels on the final image. The raw data from each exposure were reduced and combined with the MUSE pipeline v1.4 (Weilbacher et al. 2012) run under the ESOREFLEX environment (Freudling et al. 2013). The final cubes were split into 3801 single layers (i.e. single frames), sampling the targets from 4600.29 to 9350.29 Å with a step in wavelength of 1.25 Å.

The modest degree of crowding in our data allowed us to extract the background-subtracted flux of any source from every single layer of the cube using a standard aperture photometry routine with the task PHOT of IRAF. A master list of objects was created by searching for individual sources with significant peaks ($>5\sigma$ above the background): (a) in an image obtained by collapsing few frames located around the Hα line, and also (b) in an image obtained by collapsing the entire cube into a single frame, and then merging together the two lists. This approach allowed us to recover either sources dominated by Hα emission or by the stellar continuum. The extraction of the spectra was performed using an aperture of radius = 5 pixels, i.e. ∼1.5 × FWHM. A larger aperture of 10 pixels was also adopted for flux calibration purposes. With this method we extracted the spectra of 68 and 45 sources in the MB and SB, respectively. Further analysis revealed that only 26 (12) of them can be reliably associated with MB (SB), the remaining ones being background galaxies or sources lacking spectral features allowing a reliable velocity estimate. These 26 + 12 = 38 bona fide SECCO 1 sources, listed in Table 1, have spectra typical of H II regions and are the subject of the following analysis. It cannot be excluded that some of the listed sources are not independent individual H II regions but are in fact emission peaks within larger complexes. For the purpose of the present analysis, this does not seem to be a serious concern. A complementary view not based on integrated spectra of individual sources but on a pixel-by-pixel analysis will be presented in a forthcoming paper (Magrini et al., in preparation). In Fig. 1, we show two illustrative examples of the 1D spectra extracted from the MUSE cubes, bracketing the range of signal-to-noise ratio (S/N) where we were able to derive reliable metallicity estimates (see Section 4). The superb sensitivity of MUSE, the possibility to integrate the entire flux of each source inherent to 2D spectrographs, and the lack of any slit-alignment issue (that plagued B15b observations) makes the quality and the S/N of the MUSE spectra presented here much higher than those analysed in B15b (see their fig. 2 for comparison). Moreover, the spectral range covered by MUSE spectra is much wider than in B15b, e.g. including Hβ, which was not reached in B15b spectra. All these factors imply a significant improvement in the precision and reliability of the new metallicity estimates for sources of similar luminosity, with respect to that analysis (see Section 4, for further discussion).

Table 1. Position and velocity for SECCO1 H II regions.

Name	RA_{J2000} (°)	$Dec._{J2000}$ (°)	V_r^a (km s^{-1})	N_l^b	Hα flux^c (10^{-18} erg cm^{-2} s^{-1})
MB14	185.47292	13.45734	− 171 ± 7	2	29.7 ± 4.5
MB15	185.47360	13.45784	− 176 ± 11	3	54.9 ± 5.7
MB25	185.47537	13.46103	− 154 ± 4	7	319.3 ± 19.0
MB26	185.47644	13.46143	− 152 ± 8	3	171.6 ± 11.6
MB27	185.47583	13.46145	− 152 ± 5	7	296.9 ± 17.8
MB28	185.47683	13.46176	− 151 ± 6	5	61.3 ± 6.1
MB29	185.47600	13.46184	− 152 ± 6	7	218.9 ± 13.9
MB30	185.47559	13.46189	− 152 ± 5	6	226.4 ± 14.3
MB31	185.47440	13.46191	− 154 ± 4	2	33.3 ± 4.7
MB32	185.47605	13.46241	− 153 ± 9	3	43.4 ± 5.2
MB33	185.47515	13.46244	− 151 ± 8	4	78.2 ± 6.9
MB34	185.47470	13.46269	− 151 ± 30	1	26.9 ± 4.3
MB38	185.47599	13.46325	− 160 ± 30	1	15.3 ± 3.8
MB39	185.48480	13.46324	− 167 ± 30	1	9.1 ± 2.5
MB56	185.47591	13.46160	− 153 ± 4	7	259.3 ± 16.0
MB57	185.47710	13.46022	− 159 ± 30	1	11.2 ± 3.6
MB58	185.47473	13.45869	− 169 ± 30	1	35.9 ± 4.8
MB59	185.47516	13.46063	− 157 ± 6	7	233.3 ± 14.7
MB60	185.47386	13.46140	− 162 ± 30	1	23.2 ± 4.2
MB61	185.47513	13.46149	− 152 ± 5	7	266.6 ± 16.3
MB62	185.47534	13.46228	− 143 ± 7	5	104.6 ± 8.2
MB63	185.47349	13.45754	− 156 ± 10	3	64.7 ± 6.2
MB64	185.47299	13.45942	− 211 ± 15	3	26.0 ± 4.3
MB65	185.47556	13.45894	− 143 ± 11	2	59.3 ± 6.0
MB66	185.47582	13.45961	− 151 ± 30	1	33.4 ± 4.7
MB68	185.47523	13.46229	− 148 ± 7	5	97.9 ± 7.9
SB01	185.48451	13.48588	− 153 ± 6	6	170.7 ± 11.5
SB02	185.48465	13.48644	− 151 ± 7	6	185.3 ± 12.3
SB03	185.48285	13.48419	− 134 ± 11	4	109.5 ± 8.5
SB33	185.48427	13.48577	− 152 ± 12	3	113.9 ± 8.7
SB34	185.48272	13.48436	− 126 ± 11	4	102.7 ± 8.1
SB35	185.48314	13.48445	− 121 ± 12	4	90.6 ± 7.5
SB36	185.48105	13.48392	− 126 ± 15	3	54.1 ± 5.7
SB38	185.47995	13.48273	− 116 ± 11	3	99.5 ± 8.0
SB39	185.48163	13.48259	− 123 ± 9	5	169.9 ± 11.5
SB41	185.48058	13.48202	− 133 ± 8	5	154.8 ± 10.7
SB42	185.48046	13.47975	− 134 ± 30	1	13.2 ± 3.7
SB45	185.48455	13.48620	− 150 ± 6	6	193.3 ± 12.7

Notes. [a]Heliocentric radial velocity.
[b]Number of emission lines used to estimate the radial velocity.
[c]Observed flux, not extinction corrected.

The left-hand panels of Fig. 2 show stamp-size Hα images of SECCO 1 MB and SB obtained from the MUSE cube. It is clear that, in addition to several individual sources (likely H II regions), there is also diffuse hot gas emitting in Hα. In the right-hand panels, we show the corresponding portions of the combined *F606W* (t_{exp} = 2196 s) and *F814W* (t_{exp} = 2336 s) images from the *HST* GO-13735 programme (PI: Sand), which we retrieved from the STScI archive. These images resolve many of the structures seen in the Hα images into individual bright and very blue compact sources. The correspondence between the sources identified in the MUSE image and those seen in the ACS ones is excellent. We note that four SB sources are superposed on the prominent background disc galaxy at the upper margin of the image in the lower right-hand panel of Fig. 2. The lines of this galaxy (at $z = 0.187$), as well as those of the more distant smaller spiral at the lower end of its disc (at $z = 0.752$), are both seen in the spectra of these SB sources, a remarkable case of multiple chance superposition. No underlying overdensity of old stars (i.e. red giant branch stars, with age $\gtrsim$2 Gyr) associated with SECCO 1 is readily visible in the ACS image, in agreement with the conclusions by B16.

3 RADIAL VELOCITY

We derived the radial velocity of each individual compact source by determining the wavelength shift of the available emission lines relative to their rest wavelengths. To estimate the peak of each emission line, we used a Gaussian fitting algorithm. The final radial velocity was obtained from the average wavelength shift; the velocity uncertainties, given by the rms divided by the square root of the number of measured lines, encompass the range $\simeq$2–30 km s^{-1}, with an average value of $\simeq$10 km s^{-1} (see Table 1).

In Table 2, we report the mean velocity and metallicity of SECCO 1 MB and SB, separately, and the velocities of the associated H I clouds, from A15, for comparison. The reported mean velocities and velocity dispersions have been computed with a maximum-likelihood (ML) algorithm that finds the most likely parameters of a Gaussian model taking into account (and correcting for) the effects of the errors on individual velocities, following Martin et al. (2007). The small difference in mean velocity (27 ± 3 km s^{-1}, to be compared with the velocity dispersion of the LVC, σ_{LVC} = 208 km s^{-1}, Boselli et al. 2014) implies that MB and SB are indeed physically associated. MB and the AGV 226067 H I cloud have compatible systemic radial motions; the same is true for SB and AGC 229490, in spite of the spatial offset between the two systems. On the other hand, we cannot exclude a small ($\lesssim$10 km s^{-1}) but real mismatch between the systemic velocity of the MB and SB H II regions and the corresponding H I clouds, as the small spatial offset between SB and AGC 229490 may suggest ongoing ejection of the neutral gas from their stellar counterparts. The velocity dispersion of the two stellar systems is only marginally resolved in our data. This may be partly due to the contamination among spectra of overlapping sources, especially in the densest region of MB, which can result in spurious correlations of velocities. Moreover, we have excluded from the ML analysis one source from the MB sample and four sources from the SB sample, having discrepant velocities (see below). If we compute the unweighted mean and standard deviation from all the measured sources, we obtain $\langle V_r \rangle$ = −157.7 km s^{-1} and σ = 13.5 km s^{-1} for MB, and $\langle V_r \rangle$ = −134.9 km s^{-1} and σ = 13.3 km s^{-1} for SB, leaving substantially unchanged the above conclusions and indicating that the true dispersion should be similar to that measured in H I. The isolated source at $(X,Y)_{kpc} \simeq (-2.5, 0.5)$ provides significant support to the hypothesis that a few additional components associated with SECCO 1 are indeed present to the east of MB, as suggested by B16.

The left-hand panel of Fig. 3 shows that the H II regions within MB display a weak velocity gradient very similar to that displayed by the H I (A15). In general, the overall velocity fields traced by the H II regions and by the neutral hydrogen are remarkably similar, within the uncertainties. A direct comparison is presented in Fig. 4, where our sources are superimposed on the north–south position–velocity slice we derived from the A15 data (kindly provided by E. A. K. Adams). A few sources do not follow the general pattern, including, e.g. the source with $V_r < -205$ km s^{-1} at $(X,Y)_{kpc} \simeq (1, -1)$, and the four SB sources superposed on a background spiral at $(X,Y)_{kpc} \simeq (-2.5, 7)$. It is interesting to note that these velocity outliers seem to have H I counterparts, albeit of weak intensity. To check the significance of these sources, we used 3DBarolo (Di Teodoro & Fraternali 2015) to run a source detection in the H I data cube. The only two sources detected at high resolution with reliable sensitivities (thresholds between 2.5 and 3.0σ_{rms} were Secco 1 MB

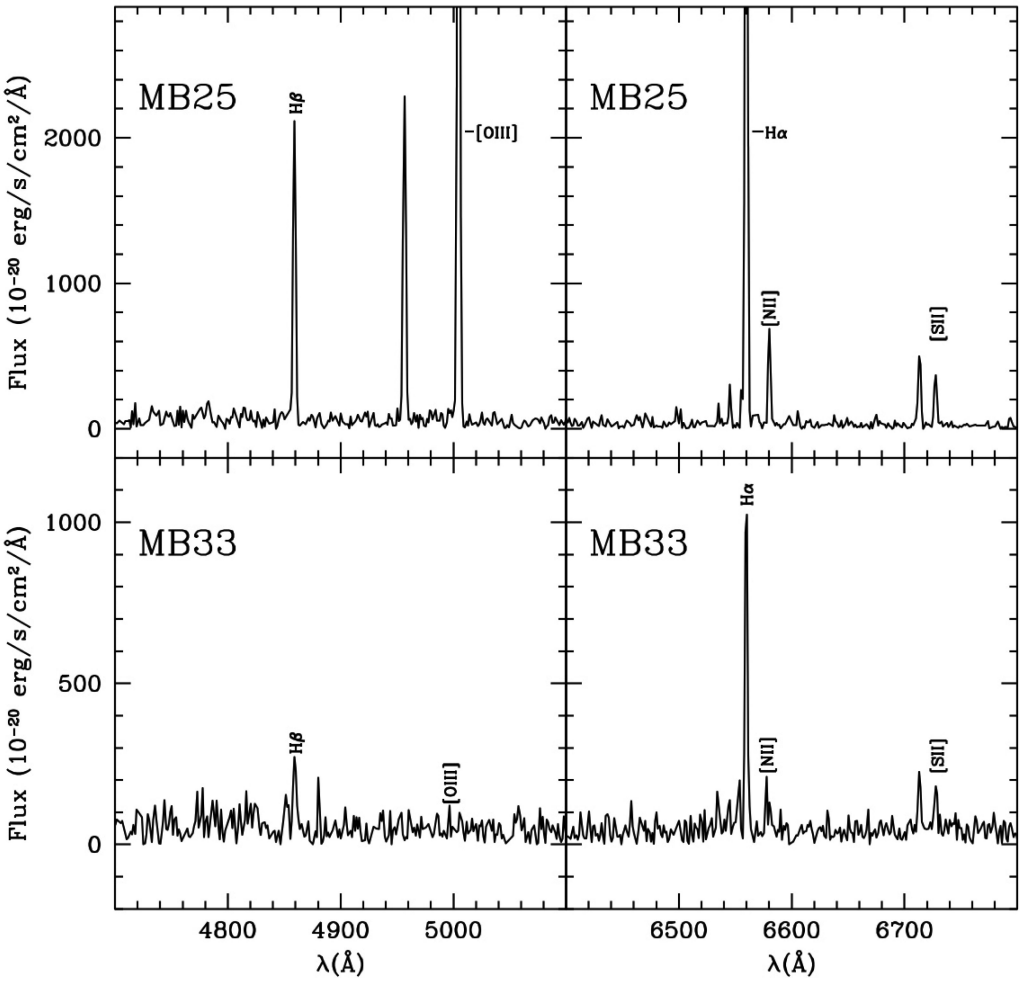

Figure 1. Portions of the extracted spectra of two compact sources identified in the MUSE data, namely MB25 and MB33, having the highest and lowest S/N, respectively. The name of the source is indicated in the plots and follows the nomenclature adopted in Table 1. Some of emission lines are labelled.

and a cloud with a much smaller velocity ($v_r = -65.6\,\mathrm{km\,s^{-1}}$ at RA = 185.466 an Dec. = 13.459) probably belonging to the Milky Way environment, if real. At lower spatial resolution (>60 arcsec) more sources are found, some emission appears in the region of the SB and farther out with some hint of a general gradient in velocity. However, it is very hard with these data to assess its reliability.

4 METALLICITY

All measured line intensities were corrected for extinction computing the ratio between the observed and theoretical Balmer decrements for the typical conditions of an H II region (see Osterbrock & Ferland 2006). In a few cases, where the extinction constant is negative, we assumed a null extinction. The extinction in both the MB and SB is quite low, with average $c\beta$ in the MB and SB equal to 0.29 ± 0.24 and 0.22 ± 0.26, respectively. We measured the line fluxes with the task SPLOT of IRAF. In the MUSE spectral range, we measured recombination lines of H (Hα and Hβ) and collisional lines of several ions ([O III], [N II], [S II], and in a few cases [O II], [Ar III], and [S III]). All the diagnostic plots based on the ratios between available lines consistently classify all the identified sources as H II regions. The fluxes of the lines that were used for the estimate of the metallicity are presented in Table 3, in a scale where the flux of H β is conventionally set to 100. The conversion to physical units can be obtained with the H α fluxes provided in Table 1, as some sources lack a reliable estimate of the H β flux.

Due to the absence of electron-temperature diagnostic lines, the gas-phase oxygen abundance of each source is determined with three different *strong-line* ratios: N2 = [N II]/Hα, O3N2 = ([O III]/Hβ)/([N II]/Hα) (Pettini & Pagel 2004, hereafter PP04) and O3S2N2, a combination of the line ratios R3 = ([O III](λ4959+λ5007))/Hβ, N2 and NS = ([S II](λ6717+λ6730))/Hα, also known as S2 (Pilyugin & Mattsson 2011). N2 and O3N2 from PP04 have indeed proved to be the strong-line diagnostics that give metallicity values very close to those obtained by directly measuring the electron temperature of the gas through the [O III]4363 line (see e.g. Andrews & Martini 2013). On the other hand, when [O III], [S II], [N II], Hα and Hβ are all simultaneously available with good S/Ns, we take advantage of the NS method, which allows us to estimate the ionizing field in absence of the [O II] lines and has been successfully validated against oxygen abundances computed using the electron temperature (López-Sánchez et al. 2012). Finally, we compute the average of the abundances from N2 and O3N2. We combine N2 and O3N2 to compensate for the effect of a varying ionization. We rejected all metallicity estimates, including line ratios with S/N < 3.0. Once this selection is applied, we get reliable estimates of the metallicity, at least from one indicator, for 18 sources, 10 in MB and 8 in SB.

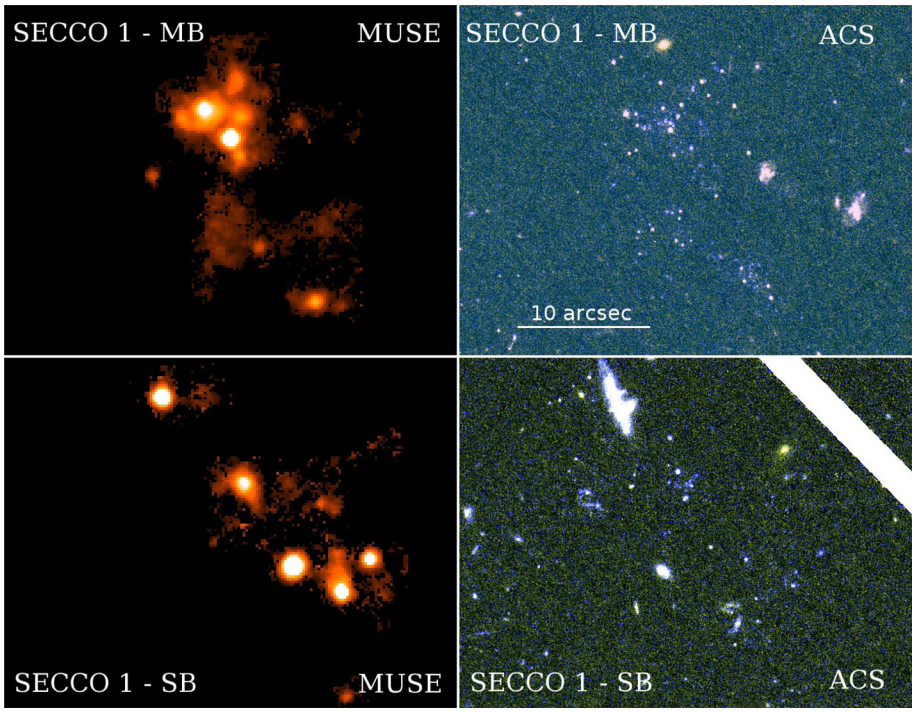

Figure 2. Left hand panels: continuum-subtracted H α images centred on the MB and SB of SECCO 1 (upper and lower panels, respectively). Right hand panels: colour image of the same field from the *F606W* and *F814W HST* images. The diagonal white band in the lower right-hand panel is the interchip gap of the camera. North is up and east to the left.

Table 2. Mean properties of stars and neutral hydrogen in SECCO 1.

Name	$\langle V_r \rangle$ (km s^{-1})	σ (km s^{-1})	Note	$\langle 12 + \log(\mathrm{O/H}) \rangle^a$	Note	V_{int}^b (mag)
SECCO 1 MB	-153.2 ± 1.4^c	3.5 ± 2.1^c	From 25 H II regions^e	8.37 ± 0.11	From 4 H II regions^d	20.9 ± 0.4
AGC 226067	-142	9 ± 3	H I (from A15)			
SECCO 1 SB	-126.5 ± 2.5^c	2.7 ± 5^c	From 8 H II region^e	8.39 ± 0.11	From 5 H II regions^d	22.0 ± 0.5
AGC 229490	-123	4 ± 2	H I (from A15)			

Notes. [a]Straight mean $\pm$ standard deviation.
[b]Integrated apparent magnitude from aperture photometry on the ACS images.
[c]Computed with a maximum-likelihood algorithm that takes into account the effect of errors on individual velocities.
[d]Only the sources where a reliable metallicity estimate can be obtained and not affected by contamination from nearby regions (see Table 4).
[e]MB: excluding MB64. SB: excluding the four most northern sources that are superposed to two background galaxies.

All the metallicity estimates from individual indicators as well as the adopted mean from different indicators are reported in Table 4, where we list also the estimates obtained from N2 and O3N2 (and their average) adopting the calibration by Marino et al. (2013), instead of Pettini & Pagel (2004). Table 4 provides all the information to evaluate the (negligible) effect of adopting one of the different indicators and/or calibrations chosen on our results. Six sources whose line ratios were found to change by varying from 5 to 10 pixels the radius of the aperture used for the flux's extraction are marked with an asterisk in Table 4, and have been excluded when computing the average metallicity obtained from estimates involving the [O III] line. In fact, the changes are small and limited to line ratios, including [O III], and are due to contamination from the two very bright adjacent sources MB25 and MB61, which have very strong [O III] lines. We verified, using the Dopita et al. (2016) diagnostic diagrams, that the higher EW([O III]) (EW = equivalent width) in these sources is not associated with metallicity effects but to an increase of the ionization parameter. A detailed discussion of the ionization conditions across SECCO 1 will be presented in a forthcoming paper (Magrini et al., in preparation). The last four rows of the table report the straight mean (Mean) and standard deviation (σ), the mean and standard deviation obtained with the same ML algorithm as used in Section 3 ($\mathrm{Mean_{ML}}$ and σ_{ML}) with the associated uncertainties, and the number of sources used to derive these parameters (N).

Note that each calibration has an intrinsic uncertainty of about $\sim$0.2 dex and that they are not exactly on the same absolute scale; it is reassuring that, nevertheless, they provide fully consistent results. In particular, the spread in metallicity is always consistent with zero, within the uncertainties: Even the straight standard deviation is smaller than the uncertainty on the individual 12+log(O/H) estimates, independently of the adopted indicator, implying a strong degree of chemical homogeneity among the various SECCO 1 sources. In the following, we will adopt metallicities from the combination of the PP04's methods as our reference values (second column of Table 4). The mean abundance from

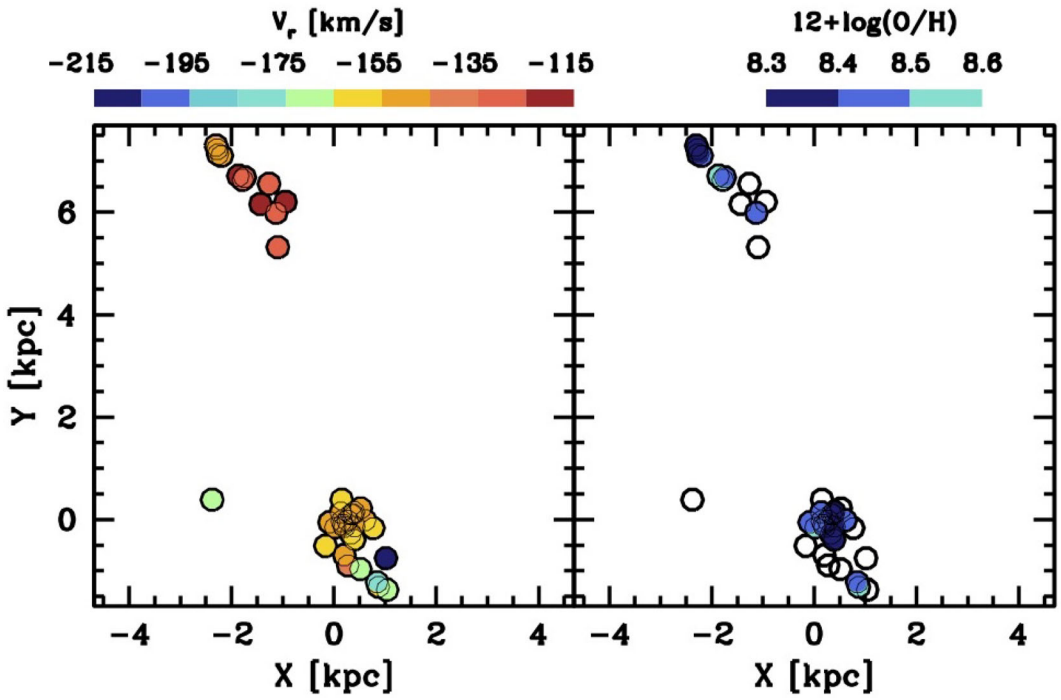

Figure 3. Left-hand panel: colour-coded velocity map for the 38 SECCO 1 MB and SB sources identified in our MUSE data. The origin of the *X*,*Y* axes is taken as the centre of MB, as derived in B15b. Right-hand panel: the same as above but with the sources colour-coded according to their metallicity. Empty circles are sources whose metallicity cannot be reliably estimated from their spectra. Note that the range of metallicity variation has an amplitude similar to the uncertainty on individual 12+log(O/H) estimates.

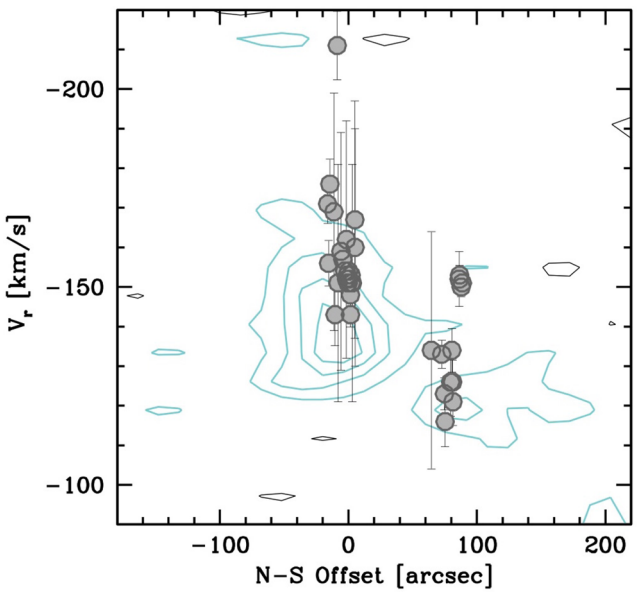

Figure 4. A position–velocity slice along the north–south direction of the H I data by A15 is compared with the velocity of the H II regions identified in this paper (grey filled circles). The H I intensity contours are plotted at −2 (black), 2, 4, 6 and 8 (green) mJy bm^{-1}.

this combination of indicators is $\langle 12 + \log(\mathrm{O/H})\rangle = 8.38$, corresponding to $0.5\,Z_{\odot}$ (assuming the solar abundance of Grevesse, Asplund & Sauval 2007). The average values for MB and SB are the same within the uncertainty, $\langle 12 + \log(\mathrm{O/H})\rangle = 8.37 \pm 0.11$ and $\langle 12 + \log(\mathrm{O/H})\rangle = 8.39 \pm 0.11$, respectively (see Table 2).

Table 3. Line flux in SECCO1 H II regions in units of the Hβ flux, set to Hβ = 100.

Name	[O III] 5007 Å	Hα 6563 Å	[N II] 6584 Å	[S II] 6717 Å	[S II] 6730 Å
MB14	–	289 ± 20	–	–	–
MB15	73 ± 25	289 ± 40	32 ± 23	84 ± 27	33 ± 23
MB25	256 ± 16	289 ± 18	32 ± 4	33 ± 4	25 ± 4
MB26	56 ± 9	289 ± 23	52 ± 9	56 ± 9	43 ± 9
MB27	130 ± 10	289 ± 20	44 ± 6	50 ± 6	37 ± 5
MB28	68 ± 34	289 ± 60	32 ± 33	71 ± 38	34 ± 34
MB29	60 ± 7	289 ± 20	54 ± 7	55 ± 7	39 ± 6
MB30	118 ± 11	289 ± 22	52 ± 8	51 ± 8	39 ± 7
MB31	125 ± 38	289 ± 48	52 ± 34	59 ± 35	43 ± 34
MB32	51 ± 22	281 ± 33[a]	35 ± 21	85 ± 23	49 ± 22
MB33	29 ± 17	289 ± 35	19 ± 17	57 ± 19	49 ± 19
MB56	75 ± 7	289 ± 19	52 ± 6	54 ± 7	38 ± 6
MB59	238 ± 16	289 ± 18	28 ± 5	32 ± 5	26 ± 5
MB61	282 ± 18	289 ± 18	41 ± 5	37 ± 5	29 ± 5
MB62	69 ± 15	289 ± 30	58 ± 15	59 ± 15	48 ± 15
MB63	31 ± 16	289 ± 30	39 ± 17	80 ± 19	41 ± 17
MB68	70 ± 16	289 ± 33	64 ± 17	58 ± 17	48 ± 16
SB01	112 ± 12	289 ± 22	29 ± 7	23 ± 7	19 ± 7
SB02	99 ± 10	289 ± 19	27 ± 6	27 ± 6	21 ± 6
SB03	15 ± 9	289 ± 24	47 ± 11	60 ± 12	38 ± 10
SB33	136 ± 16	289 ± 27	41 ± 12	19 ± 11	24 ± 11
SB34	17 ± 9	265 ± 20[a]	26 ± 9	–	–
SB35	31 ± 12	289 ± 25	42 ± 12	55 ± 13	39 ± 12
SB41	80 ± 11	289 ± 24	41 ± 9	31 ± 9	28 ± 8
SB45	100 ± 10	289 ± 20	25 ± 6	26 ± 6	22 ± 6

Only lines used for metallicity estimates are included.
Note. [a]Negative extinction constant, null extinction assumed.

Table 4. Metallicity of SECCO1 H II regions from different indicators and calibrations.

Name Ind(Cal)	⟨12+log(O/H)⟩[a] N2+O3N2(PP04)	12+log(O/H) N2(PP04)	12+log(O/H) O3N2(PP04)	12+log(O/H) NS(PM11)	12+log(O/H) N2(M13)	12+log(O/H) O3N2(M13)	⟨12+log(O/H)⟩[b] N2+O3N2(M13)
MB25	8.33 ± 0.21	8.36 ± 0.08	8.30 ± 0.11	8.31 ± 0.18	8.30 ± 0.08	8.25 ± 0.11	8.28 ± 0.19
MB26*	8.52 ± 0.22	8.48 ± 0.10	8.57 ± 0.17	8.33 ± 0.22	8.40 ± 0.10	8.43 ± 0.17	8.41 ± 0.20
MB27*	8.43 ± 0.21	8.44 ± 0.09	8.43 ± 0.11	8.33 ± 0.17	8.37 ± 0.09	8.34 ± 0.11	8.35 ± 0.19
MB29*	8.53 ± 0.21	8.49 ± 0.08	8.57 ± 0.14	8.35 ± 0.18	8.41 ± 0.08	8.42 ± 0.14	8.42 ± 0.19
MB30*	8.47 ± 0.22	8.48 ± 0.10	8.47 ± 0.13	8.37 ± 0.20	8.40 ± 0.10	8.36 ± 0.13	8.38 ± 0.19
MB56	8.50 ± 0.21	8.47 ± 0.09	8.53 ± 0.12	8.35 ± 0.17	8.40 ± 0.09	8.40 ± 0.12	8.40 ± 0.19
MB59	8.30 ± 0.22	8.32 ± 0.10	8.28 ± 0.13	8.26 ± 0.22	8.27 ± 0.10	8.24 ± 0.13	8.26 ± 0.20
MB61	8.36 ± 0.21	8.42 ± 0.08	8.31 ± 0.11	8.36 ± 0.18	8.35 ± 0.08	8.26 ± 0.11	8.30 ± 0.19
MB62*	8.53 ± 0.25	8.50 ± 0.15	8.56 ± 0.25	8.36 ± 0.33	8.42 ± 0.15	8.42 ± 0.25	8.42 ± 0.23
MB68*	8.54 ± 0.26	8.52 ± 0.16	8.57 ± 0.26	8.46 ± 0.42	8.44 ± 0.16	8.42 ± 0.26	8.43 ± 0.23
SB01	8.37 ± 0.24	8.34 ± 0.14	8.40 ± 0.18	8.29 ± 0.35	8.29 ± 0.14	8.31 ± 0.18	8.30 ± 0.22
SB02	8.36 ± 0.23	8.31 ± 0.12	8.40 ± 0.17	8.24 ± 0.28	8.27 ± 0.12	8.31 ± 0.17	8.29 ± 0.21
SB03	9999 ± 999	8.45 ± 0.13	9999 ± 999	8.25 ± 0.28	8.38 ± 0.13	9999 ± 999	9999 ± 999
SB33	8.41 ± 0.26	8.41 ± 0.16	8.41 ± 0.22	8.29 ± 0.49	8.35 ± 0.16	8.32 ± 0.22	8.34 ± 0.23
SB34	9999 ± 999	8.33 ± 0.18	9999 ± 999	9999 ± 999	8.28 ± 0.18	9999 ± 999	9999 ± 999
SB35	9999 ± 999	8.43 ± 0.16	9999 ± 999	8.25 ± 0.33	8.36 ± 0.16	9999 ± 999	9999 ± 999
SB41	8.45 ± 0.24	8.42 ± 0.13	8.49 ± 0.19	8.34 ± 0.31	8.35 ± 0.13	8.37 ± 0.19	8.36 ± 0.21
SB45	8.35 ± 0.24	8.30 ± 0.13	8.39 ± 0.18	8.23 ± 0.30	8.26 ± 0.13	8.31 ± 0.18	8.28 ± 0.21
Mean	8.38	8.41	8.39	8.32	8.35	8.31	8.31
σ	0.06	0.07	0.08	0.06	0.06 0.05	0.04	0.05
Mean_{ML}	8.38 ± 0.07	8.42 ± 0.02	8.37 ± 0.05	8.32 ± 0.06	8.35 ± 0.03	8.30 ± 0.05	8.31 ± 0.07
σ_{ML}	0.00 ± 0.08	0.00 ± 0.03	0.00 ± 0.07	0.00 ± 0.06	0.00 ± 0.03	0.00 ± 0.05	0.00 ± 0.07
N	9	18	9	17	18	9	9

References: PP04 = Pettini & Pagel (2004); PM11 = Pilyugin & Mattsson (2011); M13 = Marino et al. (2013). The NS indicator is also known as S2.
Notes. [a]Average of the values from N2(PP04) and O3N2(PP04). Adopted as reference in the analysis.
[b]Average of the values from N2(M13) and O3N2(M13). Reported for comparison.
*[O III] flux possibly affected by contamination from nearby bright sources in $r = 10$ pixels apertures.

The mean abundance of SECCO 1 is much higher than in dwarf galaxies with a similar stellar mass (see e.g. Lee, Grebel & Hodge 2003, and B15b), being more typical of galaxies as conspicuous as M33 (Magrini et al. 2010) or the Large Magellanic Cloud (Pagel et al. 1978; Carrera et al. 2008). It is also interesting to note that the observed abundance of SECCO 1 H II regions is significantly higher than the hot intracluster medium at the same projected distance from the centre of Virgo ($\simeq$0.1 $Z_{\odot}$, Urban et al. 2011).

In the right-hand panel of Fig. 3, the sources for which a reliable estimate of the metallicity can be obtained are colour-coded according to their 12 + log (O/H) values. The map illustrates very clearly the chemical homogeneity of all the sources, already noted above, with no detectable trend with position or velocity.

5 STELLAR MASS AND STAR FORMATION RATE

The very irregular morphology of SECCO 1 as well as the lack of detection of an underlying unresolved population makes the estimate of the integrated luminosity quite challenging. Our MUSE data give us an unprecedented capability of distinguishing sources that are members of SECCO 1 from unrelated background galaxies over the whole extension of the system. This factor, coupled with the use of deep high-resolution ACS images, allows us to obtain a new estimate of the total luminosity of SECCO 1 that is much more robust and reliable than previous ones (e.g. B15b, A15). We used the APT (Aperture Photometry Tool; Laher et al. 2012) to estimate the total (sky-subtracted) flux within a few non-overlapping circular apertures of different radii (∼5–10 arcsec) properly placed to enclose all the MB and SB sources and their surroundings while avoiding contamination by nearby background sources (mainly distant galaxies). The sky was estimated as the median value over wide annuli surrounding each aperture. The resulting *F606W* and *F814W* integrated magnitudes were transformed into *V* magnitudes using equation (1) of Galleti et al. (2006). We obtain $V_{\text{int}} = 20.9 \pm 0.5$ and $V_{\text{int}} = 22.0 \pm 0.5$ for MB and SB, respectively. The *F606W* − *F814W* colours are $\simeq 0.1 \pm 0.5$ and $\simeq 0.0 \pm 0.5$, respectively. Adopting $E(B-V) = 0.048$ from B15a and $D = 17.0 \pm 1.0$ Mpc, the absolute magnitudes are $M_V = -10.4 \pm 0.4$ and -9.3 ± 0.5 for MB and SB, respectively, corresponding to $L_V = 1.2^{+0.5}_{-0.4} \times 10^6 L_{V,\odot}$ and $L_V = 4.4^{+2.6}_{-1.6} \times 10^5 L_{V,\odot}$; the total *V* luminosity of SECCO 1 (MB + SB) is $L_V = 1.6^{+0.6}_{-0.4} \times 10^6 L_{V,\odot}$. The new M_V value for MB is one full magnitude fainter than what obtained by B15b and 0.7 mag fainter than that reported by A15,[3] with the same assumptions on distance and reddening. The difference is due to the removal of the contribution of background sources from the luminosity budget of SECCO 1, which was not possible with the data available to B15a or A15. Note, however, that because of the considerable uncertainty associated with these measures, the newly derived value is within $\leq 2\sigma$ of previous estimates.

From the above numbers and the new H I mass estimates by A15, considering only the spatially coincident AGC 226067 H I cloud and assuming a 10 per cent error in $M_{\text{H I}}$, we obtain, for the MB of SECCO 1, $\frac{M_{\text{H I}}}{L_V} = 12.5^{+6.5}_{-4.5}$. A similar ratio is obtained considering SB and AGC 229490, but given the spatial offset between the two systems, it is unclear how meaningful $\frac{M_{\text{H I}}}{L_V}$ is in this specific case.

The fact that all the detected sources are H II regions implies that the stellar population largely dominating the light from SECCO

[3] Converted from M_g and $(g-i)_0$ with the equation $V = g - 0.390(g-i) - 0.032$, derived in the same way as equations (5) and (6) by Bellazzini et al. (2011), and valid for $-0.6 \leq g - i \leq 2.0$.

1 has an age $\lesssim$30 Myr. There is general consensus that such a population should have a stellar M/L_V ratio $\lesssim$0.1, with M/L_V decreasing for younger ages. For example, the models by Maraston (1998) predict $M/L_V = 0.09513$ for a simple stellar population of age = 30 Myr with [Z/H] = −1.35, and $M/L_V = 0.09170$ for [Z/H] = −0.33, assuming a Salpeter (1955) initial mass function (IMF). The corresponding numbers for a Kroupa (2001) IMF are $M/L_V =$ 0.06205 and 0.05957. The BASTI solar-scaled models (Pietrinferni et al. 2004; Percival et al. 2009) predict $M/L_V = 0.061(0.083)$ for SPSS with age = 30 (50) Myr and [Fe/H] = −0.66, and $M/L_V =$ 0.067(0.085) for [Fe/H] = −1.49. $M/L_V \simeq 0.06(0.09)$ for SPSS with age = 30 (50) Myr is also predicted by the widely used Bruzual & Charlot (2003) models, with negligible dependence on metallicity and on the adopted set of stellar models (see e.g. their figs 1 and 2). Assuming, conservatively and for simplicity, $M/L_V = 0.1$, we obtain a stellar mass $M_\star \simeq 1.2 \times 10^5$ M$_\odot$ for MB and $M_\star \simeq 1.6 \times 10^5$ M$_\odot$ for the whole SECCO 1 system.

Given the very low stellar mass, the number of H II regions found in SECCO 1 may appear quite large, if taken at face value (but see Section 2). For example, the relatively large dIrr WLM has a stellar mass $M_\star = 4.3 \times 10^7$ M$_\odot$ and an H I mass $M_{\rm H\,I} = 6.1 \times 10^7$ M$_\odot$ (McConnachie 2012), and it hosts 'only' 21 H II regions (Hodge & Miller 1995). We verified that the observed number of H II regions in SECCO 1 does not imply an anomalous IMF. Adopting, conservatively, an IMF as bottom-heavy as the Salpeter (1955) one, a population with a stellar mass of $M_\star \simeq 1.6 \times 10^5$ M$_\odot$ is expected to produce ≃800 stars with $m \geq 10$ M$_\odot$, more than sufficient to populate all the observed H II regions.

On the other hand, integrating the extinction-corrected Hα luminosity over all the 38 H II regions and adopting the calibration by Kennicutt (1998), we obtain a total star formation rate (SFR) of 7.2×10^{-2} M$_\odot$ yr^{-1}.[4] This is significantly higher than the typical SFR observed in dwarf galaxies of comparable luminosity ($\simeq 1.0 \times 10^{-3}$ M$_\odot$ yr^{-1}; James et al. 2015, see e.g. their fig. 6), suggesting that the ongoing star formation episode that made SECCO 1 detectable is indeed exceptionally strong for such a low-mass system.

6 DISCUSSION AND CONCLUSIONS

From the results described above, we can draw several important conclusions shedding new light on to the nature of SECCO 1.

First of all, it is demonstrated beyond any doubt that MB and SB (and possibly also a few additional and nearly isolated H II regions in the surroundings) are physically associated. The remarkable homogeneity in metallicity strongly suggests that the various pieces of SECCO 1 originated from a single, chemically homogeneous H I cloud that is now disrupting, probably because of its interaction with the cluster environment. This would make the system unlikely to be in dynamical equilibrium, precluding a dynamical mass estimate.

Secondly, the new observations seem to confirm, albeit with the large associated uncertainties, that the system has an extreme underabundance of stars, given its H I content, in agreement with B15b and S15, and contrary to the conclusions of A15. The stellar mass estimate obtained in Section 5 implies that the H I-to-stellar mass ratio is $\frac{M_{\rm H\,I}}{M_\star} \sim 100$, placing SECCO 1 straight in the realm of almost-dark galaxies, as defined by Cannon et al. (2015, see also Eckert et al. 2015).

[4] The much lower value reported in B15a was derived from the only two H II regions considered in that paper; hence, it was based on a severely incomplete census of the Hα luminosity of the system as a whole.

Finally, the very high mean metallicity, given the stellar mass ($M_\star \sim 1.2 \times 10^5$ M$_\odot$, for MB, and $M_\star \sim 0.4 \times 10^5$ M$_\odot$, for SB), strongly suggests that the gas from which SECCO 1 stars were born was pre-enriched elsewhere, possibly torn apart by tides from the disc of a spiral galaxy during its in-fall into Virgo. Indeed, the location of SECCO 1 in a luminosity–metallicity plot is typical of tidal galaxies (Sweet et al. 2014). The (apparent) lack of an old population would also be consistent with this hypothesis. The extreme SFR, given the total luminosity, may be suggestive of a star formation episode induced by some kind of interaction. As noted in B15a, there are no obvious candidate parent galaxies in the immediate surroundings of SECCO 1. An intriguing candidate, for the kind of system that can have produced SECCO 1 as a tidal galaxy, is the interacting pair NGC 4299 + NGC 4294 (Chung et al. 2009), which show prominent H I tails, have velocity and distance compatible with membership to the LVC, and lie at a projected distance of ≃600 kpc from SECCO 1. However, an origin from this interacting system would place the detachment of SECCO 1 about 1.2 Gyr in the past (assuming the current radial velocity difference as a reference value), implying a long travelling within Virgo/LVC before the occurrence of the first feeble burst of star formation, just a few tens of Myr ago. This simple consideration suggests that other evolutionary paths are worth to be considered for this intriguing object, which may hint at the existence of an additional class of extremely dark stellar systems. A thorough comparative discussion of an alternative hypothesis on the origin of SECCO 1 is clearly beyond the scope of the present contribution and is deferred to a future paper.

ACKNOWLEDGEMENTS

This paper is based on data obtained with the European Southern Observatory Very Large Telescope, Paranal, Chile, under the Programme 295.B-5013. Based on observations made with the NASA/ESA *Hubble Space Telescope*, obtained at the Space Telescope Science Institute, which is operated by the Association of Universities for Research in Astronomy, Inc., under NASA contract NAS 5-26555. These observations are associated with programme GTO-13735. We thank the anonymous referee for her/his very thorough reading of our manuscript, and suggestions that substantially improved our paper. We warmly thank Elizabeth Adams for kindly providing the Very Large Array H I data cube of AGC 226067. GB gratefully acknowledges the financial support by the Spanish Ministry of Economy and Competitiveness under the Ramón y Cajal Program (RYC-2012-11537). This research has made use of the SIMBAD data base, operated at CDS, Strasbourg, and of the NASA/IPAC Extragalactic Database (NED), which is operated by the Jet Propulsion Laboratory, California Institute of Technology, under contract with NASA.

REFERENCES

Adams E. K., Giovanelli R., Haynes M. P., 2013, ApJ, 768, 77 (A13)
Adams E. K. et al., 2015, A&A, 580, A134 (A15)
Andrews B. H., Martini P., 2013, ApJ, 765, 140
Bacon R. et al., 2014, The Messenger, 157, 13
Bellazzini M., Battaglia G., Ibata R., Martin N., Testa V., Cignoni M., Correnti M., 2016, A&A, 591, 56 (B16)
Bekki K., 2015, MNRAS, 454, L41
Bellazzini M. et al., 2011, A&A, 527, A58
Bellazzini M. et al., 2015a, A&A, 575, 126 (B15a)
Bellazzini M. et al., 2015b, ApJ, 800, L15 (B15b)
Boselli A. et al., 2014, A&A, 570, A69
Bruzual G., Charlot S., 2003, MNRAS, 344, 1000

Cannon J. M. et al., 2011, ApJ, 739, L22
Cannon J. M. et al., 2015, AJ, 149, 72
Carrera R., Gallart C., Hardy E., Aparicio A., Zinn R., 2008, AJ, 135, 836
Chung A., van Gorkom J. H., Kenney J. D. P., Crowl H., Vollmer B., 2009, AJ, 138, 1742
Di Teodoro E. M., Fraternali F., 2015, MNRAS, 451, 3021
Donovan Meyer J., Peek J. E. G., Putman M., Grcevich J., 2015, ApJ, 808, 136
Dopita M. A., Kewley L. J., Sutherland R. S., Nicholls D. C., 2016, Ap&SS, 361, 61
Eckert K., Kannappan S. J., Stark D. V., Moffett A. J., Norris M. A., Snyder E. M., Hoversten E. A., 2015, ApJ, 810, 166
Freudling W., Romaniello M., Bramich D. M., Ballester P., Forchi V., Garcia-Dablo C. E., Moehler S., Neeser M. J., 2013, A&A, 559, A96
Galleti S., Federici L., Bellazzini M., Buzzoni A., Fusi Pecci F., 2006, ApJ, 650, L107
Grevesse N., Asplund M., Sauval A. J., 2007, Space Sci. Rev., 130, 105
Hodge P., Miller B. W., 1995, ApJ, 451, 176
James B. L., Koposov S., Stark D. P., Belokurov V., Pettini M., Olzewski E. W., 2015, MNRAS, 448, 2687
Kennicutt R. C., Jr, 1998, ARA&A, 36, 186
Kroupa P., 2001, MNRAS, 322, 231
Laher R. R., Gorjian V., Rebull L. M., Masci F. J., Fowler J. W., Helou G., Kulkarni S. R., Law N. M., 2012, PASP, 124, 737
Lee H., Grebel E. K., Hodge P. W., 2003, A&A, 401, 141
López-Sánchez Á. R., Dopita M. A., Kewley L. J., Zahid H. J., Nicholls D. C., Scharwachter J., 2012, MNRAS, 426, 2630
Magrini L., Stanghellini L., Corbelli E., Galli D., Villaver E., 2010, A&A, 512, A63
Maraston C., 1998, MNRAS, 300, 872
Marino R. A. et al., 2013, A&A, 559, 114 (M13)
Martin N. F., Ibata R. A., Chapman S. C., Irwin M., Lewis G. F., 2007, MNRAS, 380, 281
McConnachie A. W., 2012, AJ, 144, 4
Mei S. et al., 2007, ApJ, 655, 144
Osterbrock D. E., Ferland G. J., 2006, Astrophysics of Gaseous Nebulae and Active Galactic Nuclei, 2nd ed. University Science Books, Mill Valley, CA
Pagel B. E. J., Edmunds M. G., Fosbury R. A., Webster B. L., 1978, MNRAS, 184, 569
Percival S. M., Salaris M., Cassisi S., Pietrinferni A., 2009, ApJ, 690, 427
Pettini M., Pagel B. E. J., 2004, MNRAS, 348, L59 (PP04)
Pietrinferni A., Cassisi S., Salaris M., Castelli F., 2004, ApJ, 612, 168
Pilyugin L. S., Mattsson L., 2011, MNRAS, 412, 1145
Salpeter E. E., 1955, ApJ, 121, 161
Sand D. J. et al., 2015, ApJ, 806, 95
Saul D. R. et al., 2012, ApJ, 758, 44
Sweet S. M., Drinkwater M. J., Meurer G., Bekki K., Dopita M. A., Kilborn V., Nicholls D. C., 2014, ApJ, 782, 35
Tollerud E. J., Geha M. C., Grchevic J., Putman M. E., Stern D., 2015, ApJ, 798, L21
Urban O., Werner N., Simionescu A., Allen S. W., Bohringer H., 2011, MNRAS, 414, 2101
Weilbacher P. M., Streicher O., Urrutia T. et al., 2012, Proc. SPIE, 8451, 84510B

This paper has been typeset from a TEX/LATEX file prepared by the author.